# Performance Analysis of Low-Gain Feedback for Saturated Differential Drag in a High-precision Orbit Propagator

SHOUMAN, Mohamed
Department of Aeronautics and Astronautics, Kyushu University

Bando, Mai
Department of Aeronautics and Astronautics, Kyushu University

HOKAMOTO, Shinji
Department of Aeronautics and Astronautics, Kyushu University



出版情報：Transactions of Japan Society for Aeronautical and Space Sciences. 63 (5), pp.243-247, 2020-09-04. 日本航空宇宙学会
バージョン：

Trans. Japan Soc. Aero. Space Sci.
Vol. 63, No. 5, pp. 243–247, 2020
DOI: 10.2322/tjsass.63.243

*Research Note*

# Performance Analysis of Low-Gain Feedback for Saturated Differential Drag in a High-precision Orbit Propagator*

Mohamed SHOUMAN, Mai BANDO,† and Shinji HOKAMOTO

*Department of Aeronautics and Astronautics, Kyushu University, Fukuoka, Fukuoka 819–0395, Japan*

**Key Words:** Satellite Formation Flying, Differential Atmospheric Drag, Parameterized Output Regulation Algorithm, Anti-windup Controller, Parametric Lyapunov Algebraic Equation

## 1. Introduction

The practical implementation of control algorithms using differential atmospheric drag for formation flying poses some technical issues. The main issue is the low magnitude of the atmospheric drag force at high altitudes, which is handled by using the differential atmospheric drag in low earth orbits below 600 km. The second issue is its weakness to control the normal direction to the orbital plane,[1)] which is handled by integrating it with other forces to assure full controllability in different directions.[2)] This technique was also implemented to overcome the inability to precisely track the in-plane periodic trajectories in formation flying missions.[3)] Moreover, some other practical issues affect the performance of the control action when implemented in real missions. These issues are related to the saturation of the control action and uncertainty in differential atmospheric drag, which is related to the unequal relative velocity vectors of the leader and the follower, and the uncertain values of atmospheric density and drag coefficients.[4)]

In our previous paper,[3)] we mainly designed a parameterized output regulation (POR) algorithm to track the reference trajectories of formation flying missions, and it eliminated the effects of different perturbations. The control algorithm is designed for formation flying missions subject to saturation using a combination of differential atmospheric drag and thrust. For high gains that can't satisfy the conditions of the parametric algebraic Lyapunov equation (PLAE), the assumptions of non-perturbation forces except $J_2$ and equal relative velocity in designing the POR algorithm are sufficient to handle the unmodelled perturbations and uncertainties in realistic high-performance models.

The contribution of this paper is to measure the performance of the POR control algorithm under actual space environmental conditions, applying it as the precise formulation of the differential atmospheric model. It also tries to enhance the performance by incorporating an integral part with the POR control algorithm. This is achieved by designing an integrated POR control action and an integral part with an anti-windup scheme. The stability of this system is also estimated using the PLAE theorem. The paper compares the results of POR and the new control algorithm, and illustrates its effect to enhance the performance and robustness of the POR algorithm using a high-precision orbit propagator (HPOP).

## 2. Dynamics Model of Satellite Formation Flight

In this section, the equations of the relative motion are briefly reviewed for later developments. The main equations of relative motion between the leader and the follower in a Radial-Tangential-Normal (RTN/RSW) coordinate system in which the $R$-axis is directed in the radial direction, the $W$-axis is normal to the orbital plane and the $S$-axis is in the along-track direction such that $R \times S = W$ is stated in these formulas[5,6)]

$$\begin{aligned}
\ddot{x} &= x\dot{\theta}^2 + y\ddot{\theta} + 2\dot{y}\dot{\theta} - \frac{\mu(r_c + x)}{r^3} + \frac{\mu}{r_c^2} + a_x \\
\ddot{y} &= y\dot{\theta}^2 - x\ddot{\theta} - 2\dot{x}\dot{\theta} - \frac{\mu y}{r^3} + a_y \\
\ddot{z} &= -\frac{\mu z}{r^3} + a_z
\end{aligned} \tag{1}$$

where, $r_c$ is the leader position vector, $\theta$ is the true anomaly and $r = \sqrt{(r_c + x)^2 + y^2 + z^2}$, while $x, y$ and $z$ are the components of the position vector of the follower satellite relative to the leader. It is observed from Eq. (1) that the in-plane motion ($x$–$y$ plane) and the out-of-plane motion ($z$-direction) are independent, therefore they can be stated separately. For a circular orbit and the small formation radius ($x \ll r_c$), the values of $\ddot{\theta} = 0, r \approx r_c$ and $\dot{\theta}$ are equal to the mean motion $n = \sqrt{\mu/r_c^3}$. Therefore, the equations are transformed to the Hills-Clohessy-Wiltshire (HCW) model, which was developed to incorporate $J_2$ perturbation effects and formed a Schweighart-Sedwick (SS) relative dynamics model.[7)] The in-plane motion of the SS equations is stated as follows

$$\begin{aligned}
\ddot{x} - 2nc\dot{y} - (5c^2 - 2)n^2 x &= a_x \\
\ddot{y} + 2nc\dot{x} &= a_y
\end{aligned} \tag{2}$$

where, $c = \sqrt{1 + \dfrac{3J_2R_e^2}{8r^2}(1 + 3\cos 2i)}$. Introducing the control input $\boldsymbol{u} = \begin{bmatrix} u_x & \delta\hat{\alpha} \end{bmatrix}^T$ where $u_x$ is the thrust acceleration in the $x$-direction and $\delta\hat{\alpha}$ is the atmospheric drag control action,[3)] the state space representation of these equations is presented as

$$\dot{\boldsymbol{x}}(t) = A\boldsymbol{x}(t) + B_2\boldsymbol{u}(t), \quad \boldsymbol{x}(t_0) = \boldsymbol{x}_0 \tag{3}$$


*Received 15 August 2019; final revision received 13 February 2020; accepted for publication 18 March 2020.
†Corresponding author, mbando@aero.kyushu-u.ac.jp

where, $\boldsymbol{x} = \begin{bmatrix} x & y & \dot{x} & \dot{y} \end{bmatrix}^T$ is the state vector. The state and input matrices are

$$A = \begin{bmatrix} 0 & 0 & 1 & 0 \\ 0 & 0 & 0 & 1 \\ (5c^2-2)n^2 & 0 & 0 & 2nc \\ 0 & 0 & -2nc & 0 \end{bmatrix}, \quad B_2 = \begin{bmatrix} 0 & 0 \\ 0 & 0 \\ 1 & 0 \\ 0 & B_y \end{bmatrix} \tag{4}$$

where, $B_y$ is equal to $\rho C_d \frac{A_d}{m} V_{rel}^2 \cos\alpha_0$. This control coefficient $B_y$ is derived from the main formulation of the differential in atmospheric drag between the leader and follower that is expressed by this formula

$$\begin{aligned} \Delta \boldsymbol{f}_d &= \boldsymbol{f}_{d_f} - \boldsymbol{f}_{d_l} \\ &= -\frac{1}{2}\rho_f C_{df} \frac{A_f}{m_f} \boldsymbol{V}_{rel_f} \|\boldsymbol{V}_{rel_f}\| + \frac{1}{2}\rho_l C_{dl} \frac{A_l}{m_l} \boldsymbol{V}_{rel_l} \|\boldsymbol{V}_{rel_l}\| \end{aligned} \tag{5}$$

where, the cross-sectional areas over mass for the leader and follower satellites $A_l/m_l$ and $A_f/m_f$ are designed with equal drag plate areas over mass $A_d/m$ using the following equations

$$\begin{aligned} A_l/m_l &= A_d/m \sin(\alpha_0 + \delta\hat{\alpha}) \\ A_f/m_f &= A_d/m \sin(\alpha_0 - \delta\hat{\alpha}) \end{aligned} \tag{6}$$

As for the small formation radius, the relative velocity vectors of the leader and follower satellites can be represented using a scalar and equal component in the tangential direction as

$$\boldsymbol{V}_{rel} = \begin{bmatrix} 0 & V_{rel} & 0 \end{bmatrix}^T \tag{7}$$

Finally, the assumptions of small $\delta\hat{\alpha}$,[3,8] the equal atmospheric density value $\rho$ and drag coefficient value $C_d$ are used to generate the coefficient $B_y$ for state space representation, where the atmospheric density $\rho$ is calculated using the exponential density model (CIRA 72)[6] and this formula

$$\rho = \rho_0 e^{\left(-\frac{h_{ellp}-h_0}{H}\right)} \tag{8}$$

where, $h_{ellp}$, $h_0$, $\rho_0$, and $H$ are the actual altitude, base attitude, nominal density at the base attitude, and scale height, respectively.[6]

In this paper, the leader and follower satellites are placed in a "free-orbit ellipse".[9] It is necessary to modify the initial conditions to accommodate the SS model frequency. The initial velocity components $\dot{x}_0$ and $\dot{y}_0$ for the leader and follower satellites need to be adjusted to remove the secular motion and constant offset terms due to the $J_2$ effects. The initial values of $x_0$ and $y_0$ and their derivatives for the SS model are given by

$$\begin{aligned} x_0 &= \frac{r_{rel}}{2}\cos\phi, \quad y_0 = r_{rel}\sin\phi \\ \dot{x}_0 &= n\frac{2-c^2}{2c} y_0, \quad \dot{y}_0 = -2ncx_0 \end{aligned} \tag{9}$$

where, $x_0$ and $y_0$ present the initial relative states between the leader and follower satellites. It should be noted that the initial values of in-track (tangential-direction) velocity terms for the leader and follower satellites incorporate constant offset to eliminate the secular drift concerning the reference unperturbed circular orbit, which is presented as

$$\dot{y}_{0l} = \frac{3J_2 n^2 R_e^2 \sin^2 i_r}{4kr_c} \tag{10}$$

where, $k = nc + \dfrac{3nJ_2R_e^2\cos^2 i}{2r_c^2}$.

## 3. Parameterized Output Regulation

The objective of the output regulation algorithm is to find a feedback control such that the output of the system converges to zero as time tends to infinity. This problem can be used to model asymptotic tracking as well as asymptotic disturbance rejection.[10]

The dynamic equations, including those of an exogenous system, can be stated for control input subject to saturation as follows[3]

$$\begin{aligned} \dot{\boldsymbol{x}}(t) &= A\boldsymbol{x}(t) + B_1\boldsymbol{\omega}(t) + B_2\boldsymbol{\mu}_\infty\sigma(\boldsymbol{u}(t)) \\ \dot{\boldsymbol{\omega}}(t) &= S\boldsymbol{\omega}(t) \\ \boldsymbol{e}(t) &= C\boldsymbol{x}(t) + D_{11}\boldsymbol{\omega}(t) + D_{12}\boldsymbol{u}(t) \end{aligned} \tag{11}$$

where, $A$, $B_2$, $C$, and $D_{12}$ are the state-space matrices of the classical control system, while $B_1$ and $D_{11}$ are the state and output-exogenous matrices and $S$ is the state matrix for the exogenous system. The full-information output regulation problem is solvable if, and only if, $(A, B_2)$ is stabilizable and there exist control gain matrices $\Pi$ and $\Gamma$, which satisfy the regulator equation.[10]

$$\begin{aligned} \Pi S &= A\Pi + B_2\Gamma + B_1 \\ 0 &= C\Pi + D_{12}\Gamma + D_{11} \end{aligned} \tag{12}$$

The parameter $\sigma(\boldsymbol{u}(t))$ is the normalized saturation function that assures $\|\sigma(\boldsymbol{u}(t))\|_\infty \leq 1$, where it is defined as

$$\sigma(u_i(t)) = \begin{cases} \dfrac{u_i}{\mu_{\infty_i}} & \text{if} \quad |u_i| \leq \mu_{\infty_i} \\ 1 & \text{if} \quad u_i > \mu_{\infty_i} \\ -1 & \text{if} \quad u_i < -\mu_{\infty_i} \end{cases} \tag{13}$$

The coefficient matrix $\boldsymbol{\mu}_\infty \in \mathbb{R}^{m\times m}$ represents the saturation limits for different control inputs, which is stated as follows

$$\boldsymbol{\mu}_\infty = \begin{bmatrix} \mu_{\infty_1} & & 0 \\ & \ddots & \\ 0 & & \mu_{\infty_m} \end{bmatrix} \tag{14}$$

For clarity, we assume $D_{12} = 0$. Under these conditions, admissible controller actions are given by

$$\boldsymbol{u}(t) = K_\varepsilon\boldsymbol{x}(t) + L\boldsymbol{\omega}(t) \tag{15}$$

where, the feedback gain $K_\varepsilon = -R^{-1}B_2^T P_\varepsilon$ and output signal $\boldsymbol{e}(t)$ is given by

$$\boldsymbol{e}(t) = C\boldsymbol{e}^{(A+B_2K_\varepsilon)t}\hat{\boldsymbol{x}}_0 + (C\Pi + D_{11})e^{St}\boldsymbol{\omega}_0 \tag{16}$$

For POR, we consider the state weighting matrix $Q_\varepsilon = \varepsilon P_\varepsilon$, while $\varepsilon$ is the independent control parameter.[3]

$$P_\varepsilon A + A^T P_\varepsilon - PB_2R^{-1}B_2^T P_\varepsilon = 0 \tag{17}$$

We then transform the parametric algebraic Riccati equation

(PARE) to PLAE with $A_\varepsilon = -A^T - \frac{1}{2}\varepsilon I_n$, where $R > 0$ and $I_n$ is a $n \times n$ identity matrix. The parameterized matrix $P_\varepsilon$ is approved to be the unique positive definite solution from the structure of the following parametric Lyapunov equation

$$0 = A_\varepsilon^T W_\varepsilon + W_\varepsilon A_\varepsilon + C_1^T C_1 \tag{18}$$

where, $W_\varepsilon = P_\varepsilon^{-1}$ and $C_1 = R^{-\frac{1}{2}} B_2^T$.

This solution creates a stable feedback gain $K_\varepsilon = -R^{-1}B_2^T P_\varepsilon$ while assuring the boundary of the magnitude of state feedback.[11] Moreover, the properties $Q_\varepsilon > 0$ and $dQ_\varepsilon/d\varepsilon > 0$ for any $\varepsilon \in (0, \varepsilon^*]$, where $\varepsilon^*$ is the value of $\varepsilon$ for the stability margin and $\lim_{\varepsilon\to 0} Q_\varepsilon = 0$ are the necessary conditions to prove the stability of the SS model with the POR algorithm subject to the input saturation. The control action is described by

$$\boldsymbol{u}(t) = K_\varepsilon \hat{\boldsymbol{x}}(t) + \Gamma \boldsymbol{\omega}(t) \tag{19}$$

where, $L = \Gamma - K_\varepsilon \Pi$ and $\hat{\boldsymbol{x}} = \boldsymbol{x}(t) - \Pi\boldsymbol{\omega}(t)$. The stability condition for the PLAE algorithm is defined by Theorem 1 in Saberi et al.[12]

To track $\boldsymbol{\omega}(\tau) = \begin{bmatrix} c_1 \cos\omega_r\tau & c_2 \sin\omega_r\tau \end{bmatrix}^T$, the solution to the regulator equation is explicitly given by[3]

$$\Pi = \begin{bmatrix} 1 & 0 \\ 0 & 1 \\ 0 & -\dfrac{c_1\omega_r}{c_2} \\ \dfrac{c_2\omega_r}{c_1} & 0 \end{bmatrix} \tag{20}$$

$$\Gamma = \begin{bmatrix} -\dfrac{c_1\omega_r^2 + c_1 n^2(5c^2-2) + 2c_2 nc\omega_r}{c_1} & 0 \\ 0 & -\dfrac{c_2\omega_r^2 + 2c_1 nc\omega_r}{c_2 B_y} \end{bmatrix}$$

where, $c_1$ and $c_2$ are constant values that present the magnitude of the reference signals, while $\omega_r$ is the frequency of the reference signals.

### 3.1. POR control algorithm with an integral part

The new control algorithm is designed by combining the POR and an integral controller with an anti-windup scheme. It is presented by this formula

$$\boldsymbol{u}(t) = K_\varepsilon \hat{\boldsymbol{x}}(t) + \Gamma\boldsymbol{\omega}(t) + K_I \boldsymbol{q} \tag{21}$$

The anti-windup controller is based on the conditional integration method, so the integral action is switched on or off depending on the linear range or saturation range of the integration part.[13] The internal anti-windup for conditional integration is implemented as

$$\boldsymbol{q} = \begin{cases} \displaystyle\int_0^t \hat{\boldsymbol{x}}(t)dt & \text{if} \quad |K_I\boldsymbol{q}| \le \delta_I \ \&\ |\sigma(u_i)| \le 1 \\ 0 & \text{otherwise} \end{cases} \tag{22}$$

This condition can be partially interpreted by $\sup_t\left(K_I\boldsymbol{q}\right) = \delta_I$, where $0 < \delta_I < 1$. The stability conditions of the enhanced control algorithm of the POR and the integral part are similar to the PLAE theorem conditions of the POR algorithm. The margin for the percentage of the feedback control action of the new algorithm is described by

$$\begin{aligned} \|K_\varepsilon\hat{\boldsymbol{x}} + K_I\boldsymbol{q}\|_\infty &\le \|K_\varepsilon\hat{\boldsymbol{x}}\|_\infty + \|K_I\boldsymbol{q}\|_\infty \\ &\le \|K_\varepsilon\hat{\boldsymbol{x}}\|_\infty + \delta_I \le \delta \end{aligned} \tag{23}$$

where, the closure of $\delta$ is determined by $\delta \in [0, 1]$. On the other hand, Theorem 1 illustrates $\|\Gamma\boldsymbol{\omega}\|_{\infty,T} \le 1 - \delta$, where $\|\ \|_{\infty,T}$ denotes the $L_\infty$-norm after time $T$. The limits of the $\delta$-value are illustrated to determine the margin for feedback control action $\delta_I + \|K_\varepsilon\boldsymbol{x}\|_\infty$ based on the saturation level of the thrust and differential atmospheric drag for the specific satellite parameters.[3] It should be noted that when the value of $\delta_I$ increases, the margin for the feedback output regulation control action $\|K_\varepsilon\hat{\boldsymbol{x}}\|_\infty$ decreases.

## 4. Numerical Simulation Results

This section presents the numerical simulation results of the new control algorithm implemented in the high-precision orbit propagator. The results in this section present a comparison between the POR control algorithm and the new control algorithm for stable control gains when implemented in the HPOP.

The HPOP implemented for performance testing is based on AstroLib software,[3] which incorporates high-fidelity force models and a precise numerical integrator as presented in Table 1.

The more realistic formulation of the relative velocity vectors in the RTN coordinate system using orbital elements for small formation radius is presented as follows[14]

$$V_{rel_i} = \begin{bmatrix} \dot{x}_i - y_i(nc - \omega_e\cos i_r) - z_i\omega_e\cos\theta_r\sin i_r \\ \dot{y}_i + (r_c + x_i)(nc - \omega_e\cos i_r) - z_i\omega_e\sin\theta_r\sin i_r \\ \dot{z}_i - (r_c + x_i)\omega_e\cos\theta_r - y_i\omega_e\cos\theta_r\sin i_r \end{bmatrix} \tag{24}$$

where, the subscript $i$ is an indication for the leader or follower satellites. Based on the SS model, the reference orbital elements (denoted by subscript $r$) are calculated for virtual unperturbed reference circular orbit, so the initial values of $x_0, y_0, z_0, \dot{x}_0$ and $\dot{z}_0$ for the leader satellite are equal to zero, while there is a constant term that appears in initial tangential velocity term $\dot{y}_{0l}$ of the leader satellite and all relative velocity terms affected.

The satellite parameters for numerical simulations are provided in Table 2, with the saturation value of the thrust control action $u_{max} = 1 \times 10^{-4}$ N and altitude $h_{ellp} = 350$ km. From the nature of atmospheric density, it can be estimated that the limits for $\delta$ values without the integration part for reference frequency $\omega_r = n$ are approximately equal to unity for altitudes $h_{ellp} \le 500$ km, while its values for this test case decreases dramatically above $h_{ellp} \ge 550$ km, so it will be less than 0.3 for $h_{ellp} \approx 700$ km. This illustrates that it will be difficult to incorporate the integration part with the POR control action while proving the stability of the dynamics

Table 1. Reference numerical propagation force models.

| Force models | |
|---|---|
| Geopotential | $70 \times 70$ EGM-96 |
| Drag | Exponential model $C_D = 2.2$ |
| Third-body | Solar/Lunar point masses based on Jet Propulsion Laboratory ephemerides, DE405 |
| Solar radiation | Conical shadow model, reflectivity factor $C_r = 1.2$ |
| Tidal effects | No tide forces |
| **Propagator parameters** | |
| Integrator | Runge Kutta 4th order |
| Time step | 100 s |
| Simulation period | 30 days |

Table 2. Parameters of the JC2Sat satellite.

| Parameter | Symbol | Unit | Value |
|---|---|---|---|
| Mass | $M$ | kg | 18 |
| Drag plate area | $A_d$ | $m^2$ | 0.09 |
| Drag coefficient | $C_d$ | — | 2.2 |

equations for altitudes higher than 700 km.

The control parameters used for both control algorithms are stated as follows:

1. POR control action with $\varepsilon = 8.6 \times 10^{-9}$.
2. New control action with $\delta_I = 0.3, \varepsilon = 7.7 \times 10^{-9}$.

The integral gain matrix for the integrated control is $K_I = \mathrm{diag}\,(10^{-12}, 1.2 \times 10^{-6})$.

The results in Figs. 1 and 2 show the error states of the POR combined with integrated control, which are calculated using this formula

$$\boldsymbol{e}(t_i) = \boldsymbol{x}(t_i) - \Pi\boldsymbol{\omega}(t_i), \quad t_i \in \left[t_0, t_f\right] \tag{25}$$

while the control for the POR and the integral control algorithms are calculated using Eqs. (15) and (21), respectively.

Figure 1 shows the in-plane error components using the POR control algorithm for the control gains presented in Eq. (20). It shows that the error of the stable gains of the POR algorithm shows significant performance degradation and instability in the tangential direction when implemented in the HPOP.

Figure 2 presents the results of the new control algorithm, where Fig. 2(a) illustrates a moderate improvement in the radial direction as compared to Fig. 1(a), while Fig. 2(b) states that the integral part greatly enhances the performance of the tangential direction of the POR algorithm and maintains system stability for low gains when compared to the results in Fig. 1(b). Based on the difference between the ideal formulation of the relative velocity vectors presented in Eq. (7) and the more realistic formulation presented in Eq. (24), the tangential offset value from the reference circular orbit illustrated in Eq. (10) and the difference between the relative velocity vectors create deterioration in the performance of the in-plane components. These differences create more dominant effects in the mean anomaly, which was approximately presented by the tangential direction in the in-track formulation of the circular formation flying.[15] These results also explain that the integral part improves performance degradation in the tangential direction quite well.

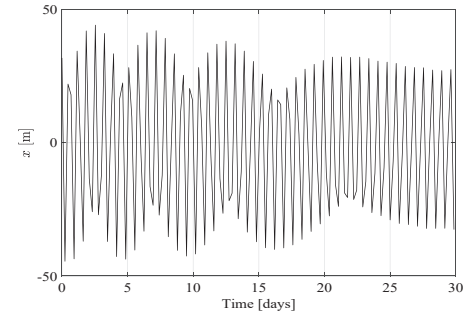


(a) Error in radial direction

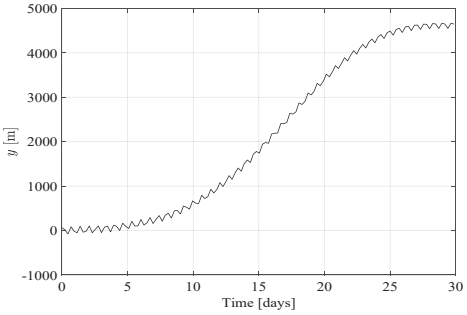


(b) Error in tangential direction

Fig. 1. Error components of the POR control algorithm.

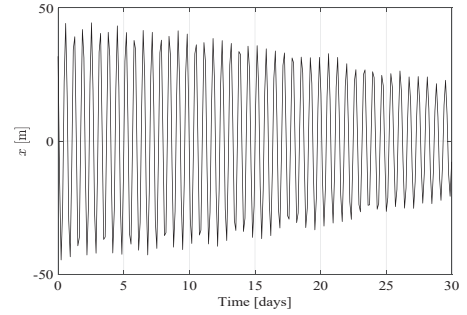


(a) Error in radial direction

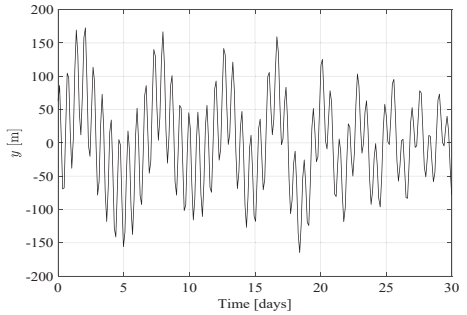


(b) Error in tangential direction

Fig. 2. Error components of the integrated control.

Figure 3 shows a comparison between the components of the control action in the POR and the new integrated control algorithms. Figure 3(a) illustrates that the values of $u_x$ for the new control algorithm are larger than POR control action in the $x$-direction and doesn't oscillate around zero as with the POR algorithm, while the error in the $x$-direction is approximately the same for both control algorithms, as presented in Figs. 1(a) and 2(a). This behavior exists due to an integral part of the new control algorithm as we strive to resolve

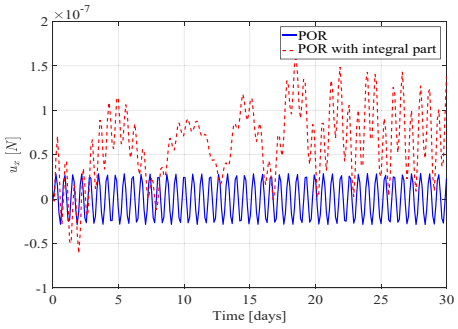


(a) $u_x$

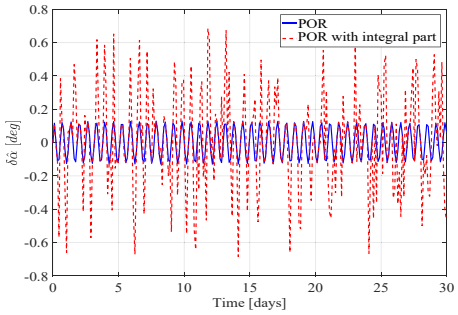


(b) $\delta\hat{\alpha}$

Fig. 3. Comparison of control components for the POR and new integrated control.

the formation maneuver problem. For the tangential direction, the control action of the new algorithm is larger than the control action of the POR algorithm, while the POR algorithm error values are higher than its values in the new algorithm and present an unstable behavior as presented in Fig. 1(b). It mainly exists because the magnitude of the integral control action is the dominant part compared to the magnitude of control action of the classical POR algorithm.

Although Fig. 2 presents a great improvement in the tangential direction results and a moderate enhancement in the radial-direction results as compared to Fig. 1, the integral part can't handle all of the perturbations and uncertainty effects in the high-precision orbit propagator models. These results reveal that the integral part with low, stable POR gains according to the PLAE approach are not sufficiently robust to deal with the unmodelled dynamics and nonlinearity of the HPOP dynamic models.

## 5. Conclusion

This paper investigated the performance of the parameterized output regulation algorithm. It proves that performance can be degraded using low stabilized control parameters according to the parametric Lyapunov algebraic equation approach. This performance degradation exists mainly due to the effects of differences between the Scheiwghart-Sedwick linear relative model and the high-precision orbit propagator nonlinear full-perturbation models. Furthermore, it is assumed in implementing construction of the parameterized algorithms that the formation radius between the leader and follower satellites is small. Therefore, this paper developed a control algorithm based on combining the parameterized output regulation algorithm and an integral control with an anti-windup scheme. The combined integral part improves the performance of the parameterized output regulation when applied in a high-precision orbit propagator. The results are promising as a first step to overcome the nonlinear and unmodelled dynamics in the formation flying problem subject to saturation. However, it can't eliminate all of the error components under different simulation conditions. We recommend testing the performance and robustness of the new algorithm against differential drag uncertainties in density and drag coefficients. It is also recommended to upgrade the control structure based on more precise relative dynamics models.

## References


1) Hajovsky, B. B.: Satellite Formation Control Using Atmospheric Drag, Ph.D. Thesis, Department of Aeronautics and Astronautics, Graduate School of Engineering and Management, Air Force Institute of Technology, USA, 2007.
2) Bevilacqua, R., Hall, J. S., and Romano, M.: Multiple Spacecraft Rendezvous Maneuvers by Differential Drag and Low Thrust Engines, *Celestial Mech. Dynam. Astronom.*, **106** (2010), pp. 69–88, doi:10.1007/s10569-009-9240-3
3) Shouman, M., Bando, M., and Hokamoto, S.: Output Regulation Control for Satellite Formation Flying Using Differential Drag, *J. Guid. Control Dynam.*, **42**, 10 (2019), pp. 2220–2232.
4) Mazal, L., Perez, D., and Bevilacqua, R.: Spacecraft Rendezvous by Differential Drag under Uncertainties, *J. Guid. Control Dynam.*, **39** (2016), pp. 1721–1733, doi:10.2514/1.G001785
5) Alfriend, K. T., Vadali, S. R., Gurfil, P., How, J. P., and Breger, L. S.: *Spacecraft Formation Flying*, Butterworth-Heinemann, Oxford, United Kingdom, 1st edition, 2010, p. 16.
6) Vallado, D. A.: *Fundamentals of Astrodynamics and Applications*, Microcosm Press, Inc, Hawthorne, CA, USA, 4th edition, 2013, pp. 388–411.
7) Schweighart, S. and Sedwick, R.: High-Fidelity Linearized J2 Model for Satellite Formation Flight, *J. Guid. Control Dynam.*, **25** (2002), pp. 1073–1080, doi:10.2514/2.4986
8) Kumar, K. D., Misra, A. K., Varma, S., Reid, T., and Bellefeuille, F.: Maintenance of Satellite Formations Using Environmental Forces, *Acta Astronautica*, **102** (2014), pp. 341–354, doi:10.1016/j.actaastro.2014.05.001
9) Alfriend, K. T., Schaub, H., and Gim, D.-W.: Gravitational Perturbations, Nonlinearity and Circular Orbit Assumption Effects on Formation Flying Control Strategies, AAS Guidance and Control Conference, Breckenridge, CO, Paper-AAS 00-012, 2000.
10) Francis, B. A.: The Linear Multivariable Regulator Problem, *SIAM J. Control Optim.*, **15** (1977), pp. 496–505, doi:10.1137/0315033
11) Zhou, B., Lin, Z., and Duan, G.-R.: Lyapunov Differential Equation Approach to Elliptical Orbital Rendezvous with Constrained Controls, *J. Guid. Control Dynam.*, **34** (2011), pp. 345–358, doi:10.2514/1.52372
12) Saberi, A., Stoorvogel, A. A., and Sannuti, P.: *Control of Linear Systems with Regulation and Input Constraints*, Springer-Verlag London, London, UK, 1st edition, 2000, pp. 69–119.
13) Yang, C., Zhang, L., and Sun, J.: Anti-windup Controller Design for Singularly Perturbed Systems Subject to Actuator Saturation, *IET Control Theory Appl.*, **10** (2015), pp. 469–476, doi:10.1049/iet-cta.2015.0189
14) Reid, T. and Misra, A. K.: Formation Flight of Satellites in the Presence of Atmospheric Drag, *J. Aerospace Eng. Sci. Appl.*, **3** (2011), pp. 64–91, doi:10.7446/jaesa.0301.05
15) Sabol, C., Burns, R., and McLaughlin, C. A.: Satellite Formation Flying Design and Evolution, *J. Spacecraft Rockets*, **38** (2001), pp. 270–278, doi:10.2514/2.3681


Katsuhiko Yamada
*Associate Editor*